Observation of trapped-electron-mode microturbulence in reversed field pinch plasmas

J. R. Duff, Z. R. Williams, D. L. Brower, B. E. Chapman, W. X. Ding, M. J. Pueschel, J. S. Sarff, and P. W. Terry

---

Observation of trapped-electron-mode microturbulence in reversed field pinch plasmas

J. R. Duff,[1] Z. R. Williams,[1] D. L. Brower,[2] B. E. Chapman,[1] W. X. Ding,[2] M. J. Pueschel,[1] J. S. Sarff,[1] and P. W. Terry[1]

[1]*Department of Physics, University of Wisconsin-Madison, Madison, Wisconsin 53706, USA*
[2]*Department of Physics and Astronomy, University of California, Los Angeles, California 90095, USA*

Density fluctuations in the large-density-gradient region of improved confinement Madison Symmetric Torus reversed field pinch (RFP) plasmas exhibit multiple features that are characteristic of the trapped-electron mode (TEM). Core transport in conventional RFP plasmas is governed by magnetic stochasticity stemming from multiple long-wavelength tearing modes. Using inductive current profile control, these tearing modes are reduced, and global confinement is increased to that expected for comparable tokamak plasmas. Under these conditions, new short-wavelength fluctuations distinct from global tearing modes appear in the spectrum at a frequency of $f \sim 50\,\text{kHz}$, which have normalized perpendicular wavenumbers $k_\perp \rho_s \lesssim 0.2$ and propagate in the electron diamagnetic drift direction. They exhibit a critical-gradient threshold, and the fluctuation amplitude increases with the local electron density gradient. These characteristics are consistent with predictions from gyrokinetic analysis using the GENE code, including increased TEM turbulence and transport from the interaction of remnant tearing magnetic fluctuations and zonal flow. *Published by AIP Publishing.*
https://doi.org/10.1063/1.5010198

The confinement of energy, particles, and momentum in a toroidal magnetic confinement fusion reactor plasma is anticipated to be limited by plasma turbulence. In present-day tokamak and stellarator plasmas, microturbulence associated with a variety of drift waves on scales close to the poloidal gyroradius is most often thought to be responsible for turbulent transport.[1,2] Larger-scale fluctuations can degrade confinement as well. For example, in conventional reversed field pinch (RFP) plasmas, multiple tearing modes arise with overlapping magnetic islands that cause the magnetic field to become stochastic over a large volume of the plasma. Parallel streaming becomes a potent transport mechanism in this case.[3–6] Stochastic transport is also important in microturbulence.[7] Understanding and controlling turbulent transport remains a central goal for magnetic confinement fusion research, and examining the behavior of these processes in different magnetic configurations offers an effective way to develop predictive models that are robust over a wide range of plasma parameters and magnetic configuration variables.

While conventional RFP plasmas suffer tearing instability, inductive current profile control yields a ten-fold improvement in global energy and particle confinement by suppressing large magnetic fluctuations associated with tearing.[8–10] Improved confinement is also obtained in self-organizing RFP plasmas through a spontaneous transition to the quasi-single-helicity regime in which one tearing-kink mode is dominant and secondary tearing modes are reduced.[11] Once tearing is sufficiently suppressed, microturbulence could limit confinement in the RFP as it does in tokamak and stellarator plasmas. Recent gyrokinetic modeling reveals drift wave instability for the RFP configuration, with some properties distinct from those seen in tokamak

and stellarator configurations.[12–15] The critical gradient threshold for instability is larger in the RFP as a consequence of the dominant poloidal magnetic field. Zonal flows are also predicted to be much stronger, and the nonlinear up-shift for the critical gradient yields predictions for relatively smaller transport from saturated turbulence.[16,17] However, zonal flows can be weakened by magnetic fluctuations,[18,19] as originally understood in the context of the nonzonal transition of tokamak Cyclone-Base-Case ion temperature gradient (ITG) turbulence. There it was found that above a threshold in plasma β (the ratio of plasma pressure to magnetic field pressure), magnetic fluctuations associated with nonlinearly excited stable modes[20] are capable of inducing an irreversible charge loss from rational surfaces, thereby disabling zonal flows and markedly raising transport levels. In the RFP, zonal-flow disabling magnetic fluctuations do not require nonlinear excitation mechanism tied to microinstability; rather, they are present from the global instability of tearing modes, even when tearing modes are reduced to a lower level by inductive control. The inclusion of an *ad hoc* magnetic fluctuation in the gyrokinetic analysis of trapped-electron-mode (TEM) turbulence in the RFP to mimic the presence of residual tearing modes results in a reduction in zonal flows and an increase in the turbulence and transport.[14]

In this letter, we describe the first experimental evidence for trapped-electron-mode (TEM) turbulence in an RFP plasma. Inductive current profile control is used to access plasmas with reduced tearing instability in the Madison Symmetric Torus (MST)[21] RFP experiment. Density fluctuation measurements using advanced far infrared (FIR) interferometry reveal emergent fluctuations that are localized to the large-density-gradient region, propagate in the electron diamagnetic drift direction, and have $k_\perp \rho_s = 0.1$–0.2, where

$k_\perp$ is the perpendicular (toroidal) wavenumber and ρ_s is the ion sound gyro-radius. The mode amplitude exhibits a clear critical-gradient threshold in the electron density. These characteristics are consistent with gyrokinetic modeling using the GENE[22] code that predicts unstable TEMs in the strong-gradient region of the plasma ($r/a \gtrsim 0.7$). Previous work has shown that TEM turbulence is important in toka-mak and stellarator plasmas,[23–31] but the interaction of turbulence-generated zonal flows and global tearing instabil-ities is an important, new physics element exposed by gyro-kinetic studies for RFP plasmas. The measurements reported here support the importance of this interaction. A particular goal of the gyrokinetic modeling performed in conjunction with the experiment is to determine if the level of residual magnetic fluctuations required to match the transport rates is consistent with the experiment, supporting the theoretical hypothesis that residual magnetic fluctuations can signifi-cantly impact zonal flows and increase microturbulent transport.

The MST produces RFP plasmas with major radius, $R_0 = 1.5$ m, minor radius, $a = 0.5$ m, and plasma current, $I_p \lesssim 600$ kA.[21] Measurements reported here were obtained in 200 kA deuterium discharges with central-chord line-aver-aged density $\bar{n}_{e,0} = 0.6 \pm 0.1 \times 10^{19}$ m^{-3} and core electron temperature up to $T_e(0) \approx 1.0$ keV. Reduced-tearing plasmas with improved energy confinement are achieved in MST using inductive pulsed-parallel current drive (PPCD).[8,32] During PPCD, a programmed ramp of the toroidal magnetic field generates parallel induction targeted to the outer region of the plasma, and the broadening of the current density[33,34] profile reduces poloidal mode number $m = 1$ tearing modes and their associated magnetic fluctuations. The stochastic transport typical for conventional RFP plasmas is thus greatly reduced. In response, the core electron temperature nearly triples even though the ohmic heating power is simul-taneously reduced. This results in dramatically improved, tokamak-like energy and particle confinement in the RFP.[9,10]

A multi-chord, far-infrared ($\lambda = 432$ μm), laser-based heterodyne interferometer-polarimeter system is used on MST to measure profiles of the equilibrium and fluctuating electron density (as well as components of the current density and magnetic field, not discussed here).[35,36] The diagnostic consists of 11 vertically viewing, single-pass chords with hori-zontal separation $\Delta R \approx 8$ cm, covering nearly the entire plasma cross section, where (R, Z) is a poloidal plane in cylin-drical coordinates. Adjacent chords are alternately staggered 5° toroidally, allowing the measurement of the toroidal wave-length of the fluctuations using two-point correlation methods. The interferometer has a bandwidth of 1 MHz and is sensitive to toroidal wavenumbers, $k_\varphi < 1 - 2$ cm^{-1}. The ion gyrora-dius is $\rho_i \leq 2$ cm for these plasmas.

Conventional RFP plasmas exhibit density fluctuations that are strongly correlated with tearing mode dynamics, including nonlinear three-wave interactions that energize sta-ble modes and generate broadband turbulence.[37] Therefore, a broadband reduction in density fluctuations associated with tearing is anticipated with PPCD due to this correlation. Figure 1 shows ensemble-averaged frequency power spectra for line-integrated electron density fluctuations measured in
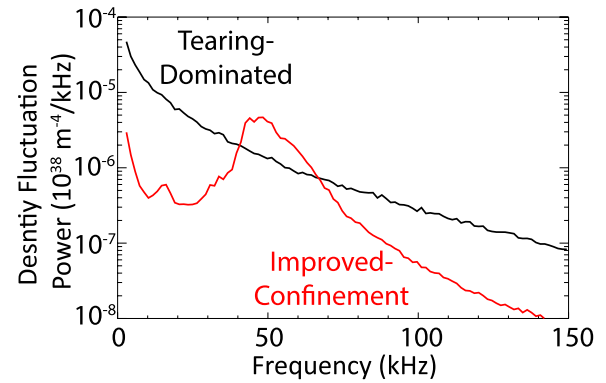
FIG. 1. Frequency power spectra for line-integrated electron density fluctua-tions in tearing-dominated (*black*) and improved-confinement (*red*) plasma conditions at impact parameter $x = 0.43$ m. The tearing-dominated spectrum is averaged over $t = 10$–11 ms, and the improved-confinement spectrum is averaged over $t = 20$–21 ms with respect to Fig. 2.

200 kA tearing-dominated and improved-confinement plasma conditions. For both regimes, the data were measured in the outer region of the plasma at an impact parameter of $R - R_0 \equiv x = 0.43$ m relative to the geometric axis, R_0. The shot-averaged fluctuation power spectrum for tearing-dominated conditions is measured in a 1 ms time window before PPCD is active and a 1 ms window near the end of the inductive control phase when the density and temperature attain their maximum values. The typical frequency range for the dominant $m = 1$, $n \gtrsim 2R_0/a$ tearing modes in the standard RFP spectrum is $f \approx 10$–30 kHz, where n is the toroidal mode number. However, the outer-chord density fluctuation spectrum for the tearing dominated regime is relatively featureless due to the contributions from many modes.[38]

As anticipated, the density fluctuations are reduced at most frequencies with PPCD, but Fig. 1 shows that a new spectral peak appears at a frequency of $f \sim 50$ kHz. These emergent fluctuations are the focus of this letter, and the measurements described below reveal that they are consistent with density-gradient-driven trapped electron modes (TEMs) predicted to be unstable in gyrokinetic modeling of PPCD plasma equilibria. The relatively narrow width of the power spectrum is similar to the "quasi-coherent" characteristic of TEM turbulence observed in several tokamak plasmas.[29,39,40]

A spectrogram for the evolution of the line-integrated density fluctuations at $x = 0.43$ m for an ensemble-average of 142 PPCD plasmas is shown in Fig. 2(a). The PPCD pro-gramming is initiated at $t = 10$ ms, which is about the time of peak I_p following plasma formation at $t = 0$. At 10 ms, the dominant density fluctuations are associated with tearing fluctuations, i.e., the "tearing dominated" spectrum in Fig. 1. As PPCD sets in, tearing fluctuations subside, and the new spectral peak forms at higher frequencies. These emergent density fluctuations are observed over the MST full range of plasma current, but the frequency spectral width of the new peak is the narrowest for 200 kA PPCD plasmas. The maxi-mum plasma pressure is obtained at the end of the PPCD control phase,[10] which is followed by a return to tearing-dominated conditions at $t > 22$ ms.

The amplitude of the emergent density fluctuations is peaked in the outer region of the plasma where the gradient
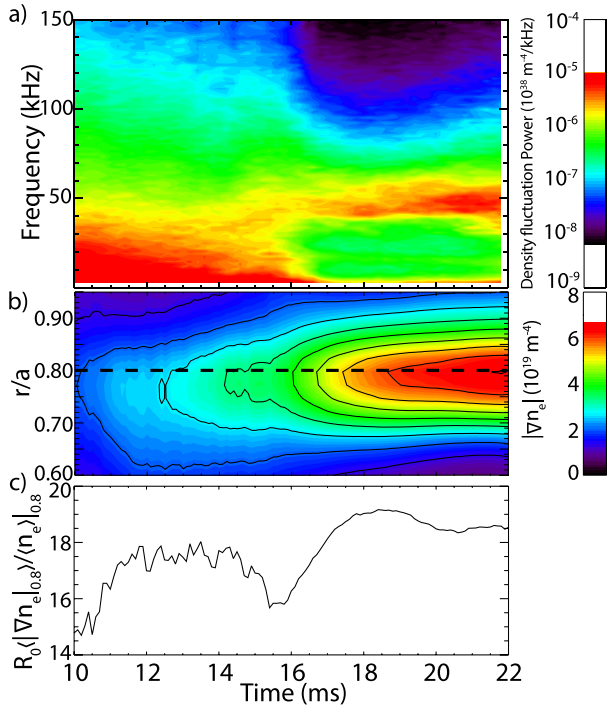
FIG. 2. Evolution of (a) the line-integrated electron density fluctuation power at $x = 0.43$ m and (b) the equilibrium density gradient for an ensemble of PPCD plasmas. The evolution of the inverse normalized density gradient scale length, $R_0\langle|\nabla n_e|_{0.8}\rangle/\langle n_e\rangle|_{0.8}$, for radius $r/a = 0.8$ is shown in (c).

in the equilibrium (flux-surface-averaged) density is the strongest. Figure 3 shows the ensemble-averaged fluctuation power of the line-integrated density fluctuations, $\langle \tilde{n}_e^2 \rangle_{x_i}$, for each interferometer chord, x_i, integrated over the frequency band 40–65 kHz to isolate the emergent fluctuations. Angle brackets $\langle\rangle$ denote an ensemble average. The ensemble average of the Abel-inverted density profiles, $\langle n_e(r) \rangle$, at 20 ms mapped to the midplane ($Z = 0$) is also plotted in Fig. 3. The time evolution of the gradient in the density calculated from the inverted profiles, $\langle |\nabla n_e(r, t)| \rangle$, is plotted in Fig. 2(b) for the outer region of the plasma, which shows that the emergence of the fluctuation coincides with an increase in $|\nabla n_e|$.
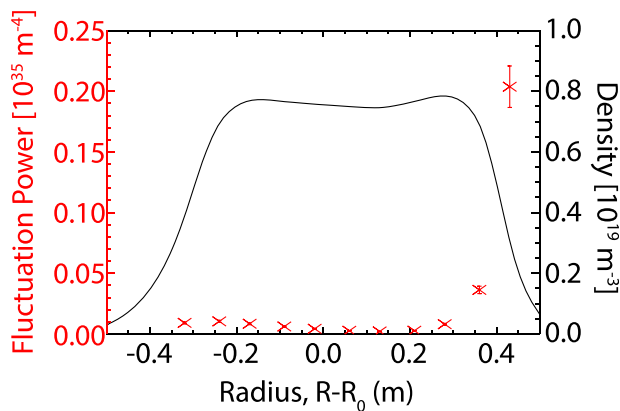
The emergent density fluctuations exhibit a clear density-gradient-threshold behavior, as shown in Fig. 4. The fluctuation power varies shot-to-shot depending on factors such as the degree of tearing suppression, which regulates increases in the plasma pressure and global confinement. The shot ensemble is binned according to the magnitude of the mean density gradient measured in each plasma, and the inverse normalized gradient scale length characteristic of the strong-gradient region, $R_0\langle|\nabla n_e|_{0.8}\rangle/\langle n_e\rangle|_{0.8}$, is calculated for each bin, where n_e and $|\nabla n_e|$ are evaluated at $r/a = 0.8$. (Note that the local density gradient scale length, $L_n \equiv n_e(r)/|\nabla n_e|$, is not a constant since the radial width of the strong-gradient region is comparable to L_n.) The power in the emergent fluctuations, $\langle \tilde{n}_e^2 \rangle$, increases when the gradient exceeds the threshold $R_0\langle|\nabla n_e|_{0.8}\rangle/\langle n_e\rangle|_{0.8} \geq 18$, as seen in Fig. 4. The time evolution of $R_0\langle|\nabla n_e|_{0.8}\rangle/\langle n_e\rangle|_{0.8}$ (averaged over the full ensemble) is plotted in Fig. 2(c), which shows the inverse gradient scale length increase over the duration of PPCD. A similar analysis for the electron temperature gradient, $|\nabla T_e|$, does not exhibit clear critical-gradient behavior although the Thomson scattering measurements in the outer region of MST plasmas presently have relatively large uncertainty due to stray laser light issues. Efforts to improve Thomson scattering are underway. Ion temperature measurements are not available for these plasmas.

The toroidal wavelength of the fluctuations is determined by the phase shift between measurements along the two outboard-most interferometer chords that are separated $5°$ toroidally ($R_0\Delta\varphi = 13$ cm). These chords are tangent to magnetic surfaces that have safety factor $q \Rightarrow 0$ and are therefore most sensitive to fluctuations with $ak_\theta \approx ak_\parallel \lesssim 1$. The two-point-correlation frequency-wavenumber power spectrum at $t = 20$ ms is shown in Fig. 5. In the $f \approx 50$ kHz range where the emergent fluctuations are the largest, the toroidal wavenumbers are $k_\varphi \approx -(0.1–0.2)\text{cm}^{-1}$, where the minus sign corresponds to wave propagation in the electron diamagnetic drift direction. This is opposite to the direction of propagation of the residual $f \sim 15$ kHz core-resonant tearing modes, $k_\varphi \approx 0.04 \text{ cm}^{-1}$ ($n \approx 6$), which acquire finite frequency from plasma flow. The density fluctuations

FIG. 3. Ensemble average of Abel-inverted density profiles on midplane at 20 ms (*black*) and ensemble-averaged amplitude of line-integrated density fluctuation frequency integrated from 40 to 65 kHz (*red*). The error bars represent one standard deviation in the data.
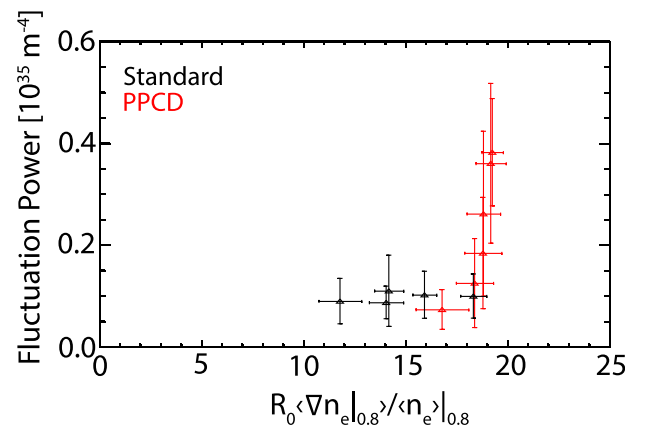
FIG. 4. Line-integrated density fluctuation power, $\langle \tilde{n}_e^2 \rangle$ (40–60 kHz), measured at $x = 0.43$ m versus inverse normalized density gradient scale length, computed at $r/a = 0.8$. The error bars represent one standard deviation in the data in both the x and y axes.
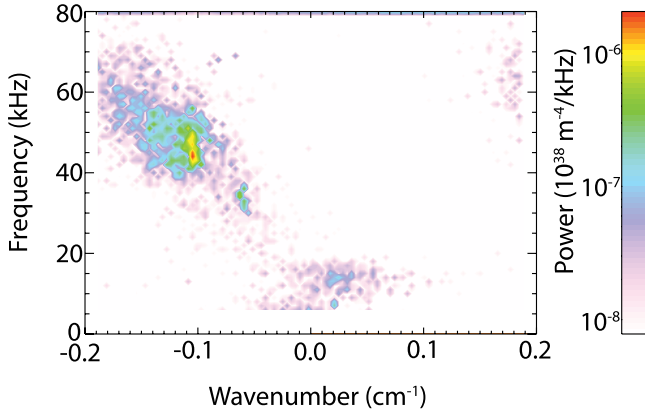
FIG. 5. Frequency-wavenumber power spectrum of the line-integrated electron density fluctuations at $x = 0.43$ m at 20 ms. The positive (negative) wavenumber corresponds to wave propagation in the ion (electron) diamagnetic drift direction.

associated with residual tearing modes are still resolved in Fig. 5. The toroidal plasma flow is small near $r/a \approx 0.8$,[41,42] and so, the Doppler shift of the emergent fluctuations is small and, if nonzero, likely to also be in the ion drift direction.

The measured features of the emergent density fluctuations are consistent with electron-branch drift waves. They exhibit a critical-gradient threshold, propagate in the electron diamagnetic drift direction, and have $k_\perp \rho_s \lesssim 0.2$, where $\rho_s \approx \rho_i \leq 2$ cm is the ion sound gyro-radius. Linear and nonlinear initial value flux-tube gyrokinetic studies are performed using the GENE code[22] with equilibrium profiles based on 200 kA PPCD plasmas. The modeled region corresponds to $r/a > 0.7$ in MST with an effective minor radial width of $\Delta r = 10\rho_s$. Linear simulations predict that the density-gradient-driven TEM is the fastest growing mode with $k_y \rho_s = 0.1 - 1.2$. The linear growth rate exhibits a critical-gradient threshold at $R_0 \nabla n/n \approx 20$, as shown in Fig. 6; this is higher than for typical tokamak equilibria by $\sim R_0/a$.[15] Nonlinear GENE simulations show the formation
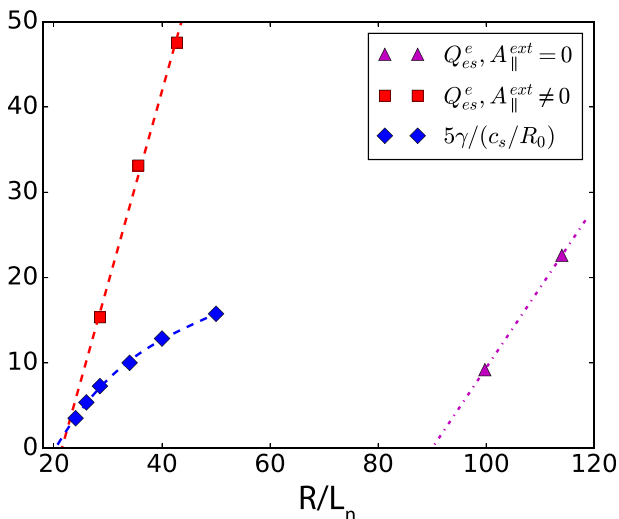
FIG. 6. (*Blue diamonds*) Linear TEM growth rates, γ, normalized to the ion sound speed crossing time, c_s/R_0; (*purple triangles*) turbulent electron heat flux, Q_{es}^e, in nonlinear simulations, normalized to $c_s \rho_s^2 n_e T_e/R_0^2$; and (*red squares*) Q_{es}^e with imposed $\tilde{B}_r/B_0 = 0.4\%$. All cases are for $r/a = 0.8$ and plotted versus the inverse density gradient scale length.

of exceptionally strong zonal flow in saturated TEM turbulence,[13] which yields a nearly five-fold nonlinear (Dimits-like[43]) upshift in the critical density gradient (Fig. 6).[17,44] The experimental density gradient is much smaller than this upshifted value, implying small TEM-generated zonal flow in the MST plasma.

Since GENE and other gyrokinetic codes are not yet capable of modeling the self-consistent interaction of multiple, nonlinearly interacting global tearing modes and microturbulence, the impact of remnant tearing modes in PPCD plasmas is modeled in GENE using an imposed, stationary magnetic perturbation, $\tilde{A}_\parallel$, with $k_x \rho_s = 0$, $k_y \rho_s = 0.2$, and a Gaussian z-profile in the flux-tube volume. The amplitude of $\tilde{A}_\parallel$ corresponds to $\tilde{B}_r/B \approx 0.4\%$, which is comparable to measured $\tilde{B}_r$ at $r/a = 0.8$. The imposed $\tilde{A}_\parallel$ is disruptive to the TEM-generated zonal flow,[14] and the turbulence saturates closer to the linear critical-gradient threshold, negating the nonlinear upshift (Fig. 6). The turbulent transport is therefore much larger when the density gradient is comparable to the experimental value. The electrostatic-fluctuation-driven electron heat flux, $Q_{es}^e \approx 15 \rho_s^2 (c_s/R_0)(L_{T_e}/R_0) n_e \nabla T_e$, for the leftmost square-symbol data point in Fig. 6 corresponds to $\chi_e \approx 20$ m^2/s using experimental parameters, close to the experimental value.

It is well documented that stochastic transport[3] associated with overlapping tearing modes is the dominant heat transport mechanism in the core of conventional MST plasmas,[4,6] and this transport is greatly reduced with PPCD. However, given the MST close-fitting conducting shell, the magnetic field is weakly stochastic in the outer region, even in conventional RFP plasmas.[45] The stochastic electron heat transport in 200 kA PPCD plasmas at $r/a \geq 0.7$ is approximately $\chi_{e,st} = v_{th,e} D_m \lesssim 2$ m^2/s, where $D_m \lesssim 4 \times 10^{-7}$ m is the estimated stochastic magnetic field diffusivity associated with the measured amplitudes of tearing modes resonant at $r/a \geq 0.7$. Previous experimental power balance measurements yield an electron heat diffusivity of $\chi_e \gtrsim 10$ m^2/s in the outer region of similar 200 kA PPCD plasmas.[9,10] This is comparable to the nonlinear GENE simulation prediction and much larger than the stochastic transport estimate. We conclude that electron heat transport from TEM turbulence is likely dominant in the edge of PPCD plasmas, but it is essential to account for the interaction with remnant tearing modes. This interaction does not rely on the magnetic field being stochastic.

In summary, density fluctuations with characteristics consistent with density-gradient-driven trapped electron modes emerge in reduced-tearing MST RFP plasmas. Gyrokinetic modeling is consistent with experimental measurements, but it is necessary to consider the impact of remnant tearing fluctuations in order to have consequential turbulent transport, which would otherwise be negligible due to exceptionally strong zonal flow. Critical gradient behavior is characteristic of microturbulence that regulates heat and particle transport, for example, the "stiffness" observed in core temperature profiles of tokamak plasmas.[28,29,46–48] The critical gradient behavior in Fig. 4 suggests the same that applies for PPCD's reduced-tearing conditions. The gyrokinetic modeling predictions for large critical gradients and

strong zonal flows show that the RFP configuration has tokamak-level turbulent transport with partial suppression of tearing modes, and it could be much smaller than for tokamak plasmas if more complete tearing reduction can be achieved.

[1] P. C. Liewer, Nucl. Fusion **25**, 543 (1985).

[2] A. J. Wootton, B. A. Carreras, H. Matsumoto, K. McGuire, W. A. Peebles, C. P. Ritz, P. W. Terry, and S. J. Zweben, Phys. Fluids B: Plasma Phys. (1989-1993) **2**, 2879 (1990).

[3] A. B. Rechester and M. N. Rosenbluth, Phys. Rev. Lett. **40**, 38 (1978).

[4] T. M. Biewer, C. B. Forest, J. K. Anderson, G. Fiksel, B. Hudson, S. C. Prager, J. S. Sarff, J. C. Wright, D. L. Brower, W. X. Ding, and S. D. Terry, Phys. Rev. Lett. **91**, 045004 (2003).

[5] W. X. Ding, D. L. Brower, G. Fiksel, D. J. Den Hartog, S. C. Prager, and J. S. Sarff, Phys. Rev. Lett. **103**, 025001 (2009).

[6] J. A. Reusch, J. K. Anderson, D. J. Den Hartog, F. Ebrahimi, D. D. Schnack, H. D. Stephens, and C. B. Forest, Phys. Rev. Lett. **107**, 155002 (2011).

[7] M. J. Pueschel, M. Kammerer, and F. Jenko, Phys. Plasmas **15**, 102310 (2008).

[8] B. E. Chapman, J. K. Anderson, T. M. Biewer, D. L. Brower, S. Castillo, P. K. Chattopadhyay, C.-S. Chiang, D. Craig, D. J. Den Hartog, G. Fiksel, P. W. Fontana, C. B. Forest, S. Gerhardt, A. K. Hansen, D. Holly, Y. Jiang, N. E. Lanier, S. C. Prager, J. C. Reardon, and J. S. Sarff, Phys. Rev. Lett. **87**, 205001 (2001).

[9] J. S. Sarff, J. K. Anderson, T. M. Biewer, D. L. Brower, B. E. Chapman, P. K. Chattopadhyay, D. Craig, B. Deng, D. J. DenHartog, W. X. Ding, G. Fiksel, C. B. Forest, J. A. Goetz, R. O'Connell, S. C. Prager, and M. A. Thomas, Plasma Phys. Controlled Fusion **45**, A457 (2003).

[10] B. E. Chapman, A. F. Almagri, J. K. Anderson, D. L. Brower, K. J. Caspary, D. J. Clayton, D. Craig, D. J. D. Hartog, W. X. Ding, D. A. Ennis, G. Fiksel, S. Gangadhara, S. Kumar, R. M. Magee, R. O'Connell, E. Parke, S. C. Prager, J. A. Reusch, J. S. Sarff, H. D. Stephens, and Y. M. Yang, Plasma Phys. Controlled Fusion **52**, 124048 (2010).

[11] R. Lorenzini, E. Martines, P. Piovesan, D. Terranova, P. Zanca, M. Zuin, A. Alfier, D. Bonfiglio, F. Bonomo, A. Canton, S. Cappello, L. Carraro, R. Cavazzana, D. F. Escande, A. Fassina, P. Franz, M. Gobbin, P. Innocente, L. Marrelli, R. Pasqualotto, M. E. Puiatti, M. Spolaore, M. Valisa, and N. Vianello, Nat. Phys. **5**, 570 (2009).

[12] I. Predebon, F. Sattin, M. Veranda, D. Bonfiglio, and S. Cappello, Phys. Rev. Lett. **105**, 195001 (2010).

[13] D. Carmody, M. J. Pueschel, and P. W. Terry, Phys. Plasmas **20**, 052110 (2013).

[14] D. Carmody, M. J. Pueschel, J. K. Anderson, and P. W. Terry, Phys. Plasmas **22**, 012504 (2015).

[15] P. W. Terry, D. Carmody, H. Doerk, W. Guttenfelder, D. R. Hatch, C. C. Hegna, A. Ishizawa, F. Jenko, W. M. Nevins, I. Predebon, M. J. Pueschel, J. S. Sarff, and G. G. Whelan, Nucl. Fusion **55**, 104011 (2015).

[16] I. Predebon and P. Xanthopoulos, Phys. Plasmas **22**, 052308 (2015).

[17] Z. R. Williams, M. J. Pueschel, P. W. Terry, and T. Hauff, Phys. Plasmas **24**, 122309 (2017).

[18] M. J. Pueschel, P. W. Terry, F. Jenko, D. R. Hatch, W. M. Nevins, T. Görler, and D. Told, Phys. Rev. Lett. **110**, 155005 (2013).

[19] P. W. Terry, M. J. Pueschel, D. Carmody, and W. M. Nevins, Phys. Plasmas **20**, 112502 (2013).

[20] D. R. Hatch, M. J. Pueschel, F. Jenko, W. M. Nevins, P. W. Terry, and H. Doerk, Phys. Rev. Lett. **108**, 235002 (2012).

[21] R. Dexter, D. Kerst, T. Lovell, S. Prager, and J. Sprott, Fusion Technol. **19**, 131 (1991).

[22] F. Jenko, W. Dorland, M. Kotschenreuther, and B. N. Rogers, Phys. Plasmas **7**, 1904 (2000).

[23] D. R. Ernst, P. T. Bonoli, P. J. Catto, W. Dorland, C. L. Fiore, R. S. Granetz, M. Greenwald, A. E. Hubbard, M. Porkolab, M. H. Redi, J. E. Rice, K. Zhurovich, and A. C.-M. Group, Phys. Plasmas **11**, 2637 (2004).

[24] Y. Xiao, I. Holod, W. Zhang, S. Klasky, and Z. Lin, Phys. Plasmas **17**, 022302 (2010).

[25] B. J. Faber, M. J. Pueschel, J. H. E. Proll, P. Xanthopoulos, P. W. Terry, C. C. Hegna, G. M. Weir, K. M. Likin, and J. N. Talmadge, Phys. Plasmas **22**, 072305 (2015).

[26] C. Deng, D. Brower, D. Anderson, F. Anderson, A. Briesemeister, and K. Likin, Nucl. Fusion **55**, 123003 (2015).

[27] H. Arnichand, J. Citrin, S. Hacquin, R. Sabot, A. Krmer-Flecken, X. Garbet, C. Bourdelle, C. Bottereau, F. Clairet, J. C. Giacalone, Z. O. Guimares-Filho, R. Guirlet, G. Hornung, A. Lebschy, P. Lotte, P. Maget, A. Medvedeva, D. Molina, V. Nikolaeva, D. Prisiazhniuk, Tore Supra, and ASDEX Upgrade teams, Plasma Phys. Controlled Fusion **58**, 014037 (2016).

[28] G. T. Hoang, C. Bourdelle, X. Garbet, G. Giruzzi, T. Aniel, M. Ottaviani, W. Horton, P. Zhu, and R. V. Budny, Phys. Rev. Lett. **87**, 125001 (2001).

[29] J. C. Hillesheim, J. C. DeBoo, W. A. Peebles, T. A. Carter, G. Wang, T. L. Rhodes, L. Schmitz, G. R. McKee, Z. Yan, G. M. Staebler, K. H. Burrell, E. J. Doyle, C. Holland, C. C. Petty, S. P. Smith, A. E. White, and L. Zeng, Phys. Rev. Lett. **110**, 045003 (2013).

[30] D. Villegas, R. Guirlet, C. Bourdelle, G. T. Hoang, X. Garbet, and R. Sabot, Phys. Rev. Lett. **105**, 035002 (2010).

[31] W. L. Zhong, X. L. Zou, C. Bourdelle, S. D. Song, J. F. Artaud, T. Aniel, and X. R. Duan, Phys. Rev. Lett. **111**, 265001 (2013).

[32] J. S. Sarff, S. A. Hokin, H. Ji, S. C. Prager, and C. R. Sovinec, Phys. Rev. Lett. **72**, 3670 (1994).

[33] J. Anderson, C. Forest, T. Biewer, J. Sarff, and J. Wright, Nucl. Fusion **44**, 162 (2004).

[34] D. L. Brower, W. X. Ding, S. D. Terry, J. K. Anderson, T. M. Biewer, B. E. Chapman, D. Craig, C. B. Forest, S. C. Prager, and J. S. Sarff, Phys. Rev. Lett. **88**, 185005 (2002).

[35] D. Brower, W. Ding, S. Terry, J. Anderson, T. Biewer, B. Chapman, D. Craig, C. Forest, S. Prager, and J. Sarff, Rev. Sci. Instrum. **74**, 1534 (2003).

[36] W. X. Ding, L. Lin, J. R. Duff, and D. L. Brower, Rev. Sci. Instrum. **85**, 11D406 (2014).

[37] L. Lin, W. X. Ding, D. L. Brower, W. F. Bergerson, T. A. Carter, T. F. Yates, A. F. Almagri, B. E. Chapman, and J. S. Sarff, Phys. Rev. Lett. **108**, 175001 (2012).

[38] N. E. Lanier, D. Craig, J. K. Anderson, T. M. Biewer, B. E. Chapman, D. J. D. Hartog, C. B. Forest, S. C. Prager, D. L. Brower, and Y. Jiang, Phys. Plasmas **8**, 3402 (2001).

[39] H. Arnichand, R. Sabot, S. Hacquin, A. Krmer-Flecken, X. Garbet, J. Citrin, C. Bourdelle, G. Hornung, J. Bernardo, C. Bottereau, F. Clairet, G. Falchetto, and J. Giacalone, Nucl. Fusion **54**, 123017 (2014).

[40] W. L. Zhong, Z. B. Shi, Z. J. Yang, G. L. Xiao, Z. C. Yang, B. Y. Zhang, P. W. Shi, H. R. Du, X. M. Pan, R. B. Zhou, L. H. Wan, X. L. Zou, M. Xu, X. R. Duan, Y. Liu, G. Zhuang, H.-A. Team, and J.-T. Team, Phys. Plasmas **23**, 060702 (2016).

[41] B. E. Chapman, A. F. Almagri, J. K. Anderson, C.-S. Chiang, D. Craig, G. Fiksel, N. E. Lanier, S. C. Prager, J. S. Sarff, M. R. Stoneking, and P. W. Terry, Phys. Plasmas **5**, 1848 (1998).

[42] D. Craig, A. F. Almagri, J. K. Anderson, J. T. Chapman, C.-S. Chiang, N. A. Crocker, D. J. Den Hartog, G. Fiksel, S. C. Prager, J. S. Sarff, and M. R. Stoneking, Phys. Rev. Lett. **79**, 1865 (1997).

[43] A. Dimits, B. Cohen, N. Mattor, W. Nevins, D. Shumaker, S. Parker, and C. Kim, Nucl. Fusion **40**, 661 (2000).

[44] D. R. Ernst, K. H. Burrell, W. Guttenfelder, T. L. Rhodes, A. M. Dimits, R. Bravenec, B. A. Grierson, C. Holland, J. Lohr, A. Marinoni, G. R. McKee, C. C. Petty, J. C. Rost, L. Schmitz, G. Wang, S. Zemedkun, L. Zeng, and DIII-D Team, Phys. Plasmas **23**, 056112 (2016).

[45] G. Fiksel, S. C. Prager, W. Shen, and M. R. Stoneking, Phys. Rev. Lett. **72**, 1028 (1994).

[46] X. Garbet, P. Mantica, F. Ryter, G. Cordey, F. Imbeaux, C. Sozzi, A. Manini, E. Asp, V. Parail, R. Wolf, and J. E. Contributors, Plasma Phys. Controlled Fusion **46**, 1351 (2004).

[47] D. Mikkelsen, H. Shirai, H. Urano, T. Takizuka, Y. Kamada, T. Hatae, Y. Koide, N. Asakura, T. Fujita, T. Fukuda, S. Ide, A. Isayama, Y. Kawano, O. Naito, and Y. Sakamoto, Nucl. Fusion **43**, 30 (2003).

[48] F. Ryter, C. Angioni, M. Beurskens, S. Cirant, G. T. Hoang, G. M. D. Hogeweij, F. Imbeaux, A. Jacchia, P. Mantica, W. Suttrop, and G. Tardini, Plasma Phys. Controlled Fusion **43**, A323 (2001).